Glass Technol.: Eur. J. Glass Sci. Technol. A, June 2013, 54 (3), 111–118

Thermal behaviour of iron aluminium phosphate glasses containing $UO_{2.67}$

D. S. Rodríguez, P. A. Arboleda, D. O. Russo*

Centro Atómico de Bariloche (CAB), Av. E. Bustillo 9500-(8400)-S. C. de Bariloche - (RN), Argentina

F. Soldera

Functional Materials, Saarland University, P.O. Box 151150, D-66041 Saarbrücken, Germany

C. J. R. González-Oliver

**C.O.N.I.C.E.T Avda. Rivadavia 1917, CP 1033 AAJ, Buenos Aires, Argentina and*
Centro Atómico de Bariloche (CAB), Av. E. Bustillo 9500 - (8400) - S. C. de Bariloche - (RN), Argentina

J. Ma. Rincón[1]

The Vitreous and Ceramics Lab/Group, IETcc, CSIC, c/ Serrano Galvache 4, Madrid - 28033, Spain

Manuscript received 6 September 2011
Revision received 28 August 2012
Manuscript accepted 30 October 2012

The thermal behaviour (viscosity variation, dilatometric and crystallization trends) of several iron aluminium magnesium phosphate glasses that contain significant amounts (6–19 wt%) of uranium oxide ($UO_{2.67}$) is presented as well as new data related to the densification of powder compacts prepared from such compositions. The sintering study of such vitreous powders can help to assess the relative capability for the immobilization and stability of the uranium oxide in these glassy or glass-ceramic matrices.

1. Introduction

For a long time, glasses have been used in nuclear science and technology; there is currently renewed interest in applications of glasses for nuclear waste immobilisation.[1] Vitrification of industrial wastes is considered a good candidate process for inertisation and/or recycling of a wide range of wastes.[2,3] In this sense the vitrification of radioactive wastes is very promising for immobilising isotopes of high and medium activity resulting from nuclear power production and applications of nuclear technology in science and industry.[4] Several glassy matrices have been investigated in last years namely borosilicate, high silica and lead iron phosphate glasses and basalt compositions.[5] Iron phosphate glasses are of growing interest due to promising properties for several applications[6] and particularly as matrices for the immobilisation of some isotopes[7–15] based on compositions with Fe^{2+}/Fe_{total}<0·4 obtained from the starting composition $40Fe_2O_3$–$60P_2O_5$, because over this ratio there are difficulties in making this type of glasses.[7] Results show that they are formed by a network of $Fe^{2+}_{(1-x)}Fe^{3+}_x(P_2O_7)_2$ groups with clusters of $(Fe_3O_{12})^{16-}$ which are interconnected with $(P_2O_7)^{4-}$ groups. It appears that their crystallisation trend and kinetics depend strongly on the oxidation states of iron.[10,18,21,23] More recently, Zhang *et al*,[15] after considering the thermal stability of glasses from the $Fe_4(P_2O_7)_3$–$Fe(PO_3)_3$ system, have reviewed the phase equilibria in the Fe_2O_3–P_2O_5 system[16] concluding that three eutectic points are present in the equilibrium diagram of this system at 58, 42·7 (925°C) and 37% mol Fe_2O_3 (907°C). The majority of glass compositions which have been investigated by the CAB research group in collaboration with the Rincón Group in Madrid (Bariloche Group, Argentina and Torroja Group in Madrid, Spain) in recent years as hosts for uranium oxide nuclear waste, due to the capability of iron phosphate glasses for immobilising transuranic elements,[17–23] are in this range.

Because of debate about the limited stability of iron phosphate glasses with the matrix composition $60P_2O_5$–$40Fe_2O_3$ it has been necessary to analyse in depth the thermal properties of this type of glasses.[11] Thus, the aim of this paper is to summarise the thermal properties of recently investigated glasses, 'AR series', with U_3O_8 additions.[23] The compositions studied extends the previously investigated range of glasses melted in pure alumina crucibles (some of them having planned additions of SiO_2) by the Bariloche Group.[21] Thermal expansion (TE), differential thermal analysis (DTA), hot stage microscopy (HSM) and dilatometric densification[17–23,32] of the glasses have been used. UO_2–Fe_2O_3–P_2O_5 glasses produced at CAB include additions of 5·1–13·71 wt% of U_3O_8 waste have been melted in Al_2O_3+MgO crucibles and

[1] Corresponding author. Email jrincon@ietcc.csic.es

also contain Na_2O. Furthermore, sintering of pellets[22] from the powdered glasses gives useful information about the capability of the iron phosphate matrices for immobilising such a waste.

2. Experimental

Tables 1 and 2 give the original batch compositions and the final analysed compositions respectively of the AR glasses obtained from the UO_2–Fe_2O_3–P_2O_5 system. These compositions have been designed starting from the AR1 glass that contains 14 wt% U_3O_8 previously studied by González Oliver *et al.*[23] The criteria for this design was to explore compositions around the location of the AR1 composition following a counter clockwise spiral as has been represented in Figure 1. Composition AR3 without UO_2 has been included as a reference in this diagram.

The glasses have been melted in a Kanthal furnace model Deltech DT-31 in 100 ml sintered alumina/magnesia crucibles following a previous calcination treatment at 700°C for 1 h. Melting was carried out at 1300°C in air at ambient pressure; the sample was heated from ambient temperature to 1200°C over a 4–6 h period, then this temperature was held for 1 h. The temperature was then increased to 1300°C over 15–30 min and finally at 1300°C the melt was poured into a grooved steel mould. For preparation of sintered glasses as pellets, part of the glass rods were crushed in a steel percussion mortar and ground in small 0·5 g portions in C_3H_7OH for 2 min in an agate mortar and pestle. The raw materials were: $AlPO_4$ (98% pure) and $NH_4H_2PO_4$ (99·5 % pure; CAAL, Brasil), Fe_2O_3 (Berna, Argentina), SiO_2, Na_2CO_3 (Cicarelli, Argentina) and U_3O_8 (Dioxitek S.A.; Comisión Nacional de Energía Atómica, CNEA).

The chemical compositions of the final glasses were obtained by energy dispersive spectroscopy (EDS) using a EDS/ EDAX detector attached to a scanning electron microscope (SEM, Philips 515) operating at 20 kV. The specimens were ground flat and polished with 5 μm diamond paste. The data was processed with internal standards by using the commercial software provided with the detector. Energy calibration in this EDS system was made using the Cu K_α line. X-ray diffraction (XRD) analysis of crystalline phases formed after heating were measured using a Philips PW 1700 diffractometer at a wavelength of λ_{CuK_α}=0·154054 nm.

Table 1. Nominal chemical composition of the float glass substrate

Elements	*wt%*	*mol%*
SiO_2	72·5	71·0
Na_2O	13·7	13·0
CaO	9·12	9·57
MgO	4·14	6·05
SO_3	0·247	0·182
Al_2O_3	0·13	0·08
Fe_2O_3	0·103	0·038
K_2O	0·04	0·03
TiO_2	0·01	0·01

Table 2. Final analysed compositions of the AR glasses

wt%	P_2O_5	Fe_2O_3	UO_2	Na_2O	Al_2O_3	MgO	P_2O_5/ Fe_2O_3	P_2O_5/ UO_2	P_2O_5/ Fe_2O_3 +UO_2
AR2	54·2	33·1	6·2	2·2	2·3	1·9	1·637	8·74	1·38
AR4	45·8	42·2	6·2	2·3	1·9	1·6	1·085	7·39	0·95
AR7	65·0	19·0	9·1	2·1	2·6	2·1	3·421	7·14	2·31
AR5	46·3	35·4	12·5	2·3	1·7	1·8	1·305	3·70	0·97
AR1	53·7	27·0	12·9	2·3	2·1	1·9	1·989	4·16	1·35
AR6	57·3	18·4	18·2	2·3	1·7	2·1	3·114	3·15	1·57

DTA runs were carried out with an Universal VII-IATA apparatus using 20 mg of glass powder placed inside Al_2O_3 crucibles (Almath crucibles, U.K.) at a heating rate of 10°C min^{-1} in static air. Linear thermal expansion (LTE) was measured with a differential vertical dilatometer (Theta Dilatronics II; USA) at heating rates of 1 and 5°C min^{-1} under flowing O_2. The alumina push rod exerted a 6 g load on the specimen (L_0~2mm; 2×4×4 mm block). The dilatometer was calibrated by inserting a 2 mm thick piece of high purity (optical fibre grade) silica glass instead of the specimen and repeating the thermal cycle. The corrected data is quoted as $\Delta L/L_0=[L(T)-L_0]/L_0$, where L_0 is the initial height of the specimen. The errors in $\Delta L/L_0$ and temperature (T) measurements are less than 3% and ±3°C, respectively.

Hot stage microscopy (HSM) used an in-house apparatus (CAB) equipped with a LCD camera for visualising the shape changes on heating of a pressed pellet produced from finely ground glass obtained from the as-cast rods.

A detailed transmission electron microscope (TEM) and SEM/EDS/electron backscattered diffraction (EBSD) study was reported in previous papers[21–23] on the structure of crystalline phases produced after controlled heating of these AR glasses. To complement the discussion here, some SEM/EBSD micrographs which were obtained by a FEI-SEM

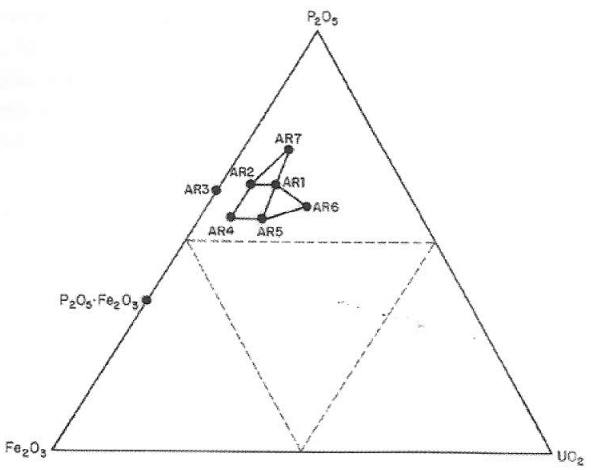

Figure 1. Location of the AR starting batch compositions in the ternary diagram: UO_2–Fe_2O_3–P_2O_5 (wt%). The phase $P_2O_5.Fe_2O_3.FePO_4$, is located at 35·32P_2O_5–64·68Fe_2O_3)

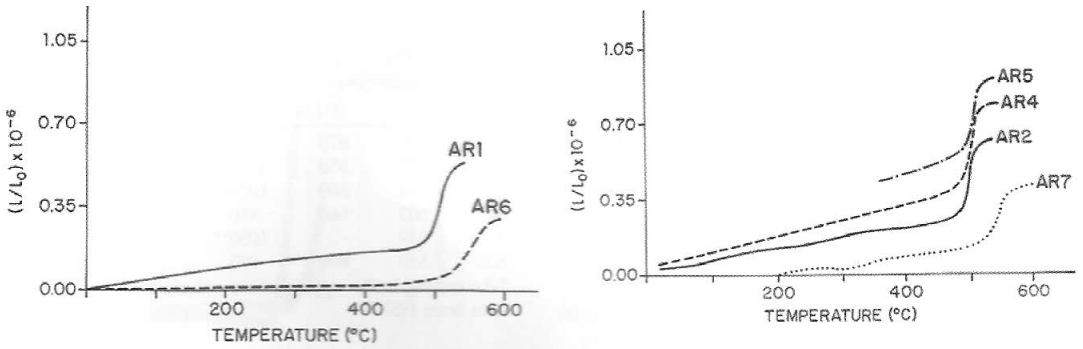

Figure 2. Thermal expansion (TE) of the AR glasses heated at 2°C min^{-1}, after annealing at the same rate, under air until softening temperature. For AR5 the valid data is from about 400°C where the cooling was reversed to a heating rate of 2°C min^{-1}

equipped with a Dual Beam FEI Strata DB 235 with Edax/TSL Orientation Imaging v5.3 EBSD system and a Hikari CCD camera.

Water leaching experiments using the DIN 38414 S4 method[24] (used previously by Romero *et al*[25] for glass ceramics produced by vitrification of hospital wastes) have been carried out. The grain size for the leaching experiments was 1–0·063 mm. The tests were conduced at ambient temperature and the glass/H_2O mix was stirred at 300 rpm for 24 h. Each sample was weighed and placed in a wide neck flask of appropriate volume, after that deionised water was added in a 1:10 ratio. After the leach test the undissolved residue was separated by filtration and the concentration of components in the filtrate was determined by inductively coupled plasma (ICP) method. This leaching test allows us to discuss the relative chemical durabilities of the glasses investigated here, although it is not the ASTM-PCT method widely used for nuclear waste forms.[26] The analysis of leached liquid was carried out by ICP and the final leaching quantity from the water residue after leaching of glass (mg/ kg) was calculated using $w_E=\beta V_E/m_s$; where β is the concentration of the element in the leachant (mg/L), V_E is the volume of filtered eluate, which in this case is 10 times the weight of the sample m_s (initial mass).

Table 3. Thermal expansion and glass transformation temperatures for AR glasses AR glass series corrected from Russo et al[21] *and melted in Al_2O_3/MgO crucibles*

Code	*Glass transition temperature, T_g*	*Softening point, T_s*	*Thermal expansion, $\alpha/10^{-7}$ °C^{-1}*
AR1	496	539	2·6
AR2	493	526	7·7
AR4	504	531	8·9
AR5	503	532	10·8
AR6	539	589	3·4
AR7	539	587	4·9

3. Results and discussion

3.1. DTA and dilatometry data. Crystallisation tendencies.

The results of dilatometry (thermal expansion coefficient, TEC) on the AR glasses are shown in the Figure 2. It can be seen that TEC for these iron phosphate glasses is in the range 2·6–10·8×10^{-6} °C^{-1}. Glass transition temperatures (T_g) are in the range 493-539°C and softening temperatures (T_s) are in the range 526–589°C.

From the DTA results (Figure 3) it can be seen that AR1, AR6 and AR7 glasses are the most stable with respect to crystallisation, with AR6 being the most stable. On the other hand, AR2, AR4 and AR5 exhibit massive crystallisation with early multiple crystallisation peaks. AR1 only exhibited surface crystallisation. These glasses have higher iron oxide contents. Table 3 gives the estimated T_g values from the DTA traces.

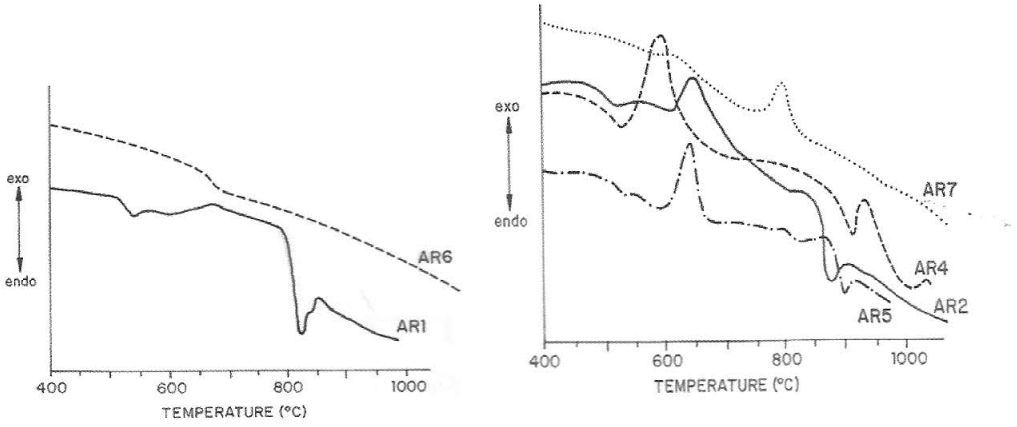

Figure 3. DTA traces for AR glasses at 10°C min^{-1} under air

AR1 and AR4 show visible (by eye) surface crystallisation, which is compatible with some internal crystallisation in the case of the AR4 glass. AR2 and AR5 have similar DTA traces reflecting the highest internal crystallisation of twinned $Fe_3(P_2O_7)_2$ crystals.[23]

Both AR2 and AR5 show two inflexions in the region of T_g which can be attributed to the presence of glass-in-glass phase separation in these glasses. This can indicate a higher tendency to internal crystallisation. These glasses are the ones with the highest iron oxide contents.

AR2, AR4 and AR7 glasses exhibit more or less intense exothermic bands,which must correspond to both pyrophosphate crystalline phases $Fe_3(P_2O_7)_2$ and $FePO_4$ detected in previous work,[23] although by sol-gel processing it was previously found that $Fe_3(P_2O_7)_2$ is produced in the 657–727°C interval and $Fe_4(P_2O_7)_3$ at higher temperatures of 797–827°C, which was not-found in this case with sintered powdered glasses.[19] Glasses with higher $UO_{2\cdot67}$ contents (AR1, AR6 and AR7) do not show the same crystallisation behaviour. Therefore, it does not seem that the presence of uranium is related to this phenomenon.

Several criteria are considered for determination of stability parameters of glasses. The debate about these methods has been reviewed and discussed very recently by Pérez *et al.*[27] Glass-forming ability (GFA) assesses the ease of vitrifying a liquid on cooling, while glass stability (GS) assesses the resistance of the glass to devitrification on heating. Several parameters proposed by different authors[26] allow the GS to be assessed namely

- Weinberg parameter: $K_W=(T_c-T_g)/T_L$
- Hrüby parameter: $K_{gl}=(T_c-T_g)/(T_L-T_c)$
- Lu-Liu parameter: $K_{LL}=T_c/(T_g+T_L)$

where T_c is the maximum of crystallisation peak temperature or the onset temperature of the crystallisation peak. To obtain the GS parameters it is recommended to use the maximum and to calculate the GFA as the onset value. In this case the temperature at the maximum of the crystallisation peak has been used. These parameters should be a guide as to the ability of the glass to form a glass-ceramic, i.e. higher GS values imply that it is more difficult to crystallise the glass during heating.

The above mentioned criteria can be followed for determination of T_c. However determining T_L by DTA or dilatometry is not easy and it is more easily determined using the fluidity point observed by HSM.[28–30] Fluidity it is considered to be the temperature when the glass shadow under HSM fully descends becoming tangential to the last scale marking of the LCD camera grating. In our experiments observation of this point has not been clear, therefore the criteria developed by Peña *et al*[30] have been used; a comparison is made of all the points observed by TE, DTA and HSM of the powdered glassy frits which define clearly the relative location of each of the transformation points. T_L is defined by the inflexion point where the highest temperature exotherm of the DTA traces starts.

Table 4. Characteristic temperatures in °C obtained from the DTA traces for the AR iron phosphate glasses uranium oxide additions

Glass code	T_g	*Crystallisation temperature,* T_{c1}	T_{c2}	*Type of crystallisation*
AR1	525	670	870	Surface
AR2	500	650	840	Bulk
AR4	520 and 600	600	950	Bulk
AR5	520 and 530	600	880	Bulk
AR6	675	-	-	No crystallisation
AR7	550	800	-	Bulk

Table 5. Glass stability (GS) parameters for the uranium iron phosphate glasses

Code	T_g *(TE)*	T_c *(DTA)*	T_L* *(HSM and DTA)*	K_{gl}	K_W	K_{LL}
AR1	496	670	950	0·62	0·18	0·41
AR2	493	650	1000	0·45	0·16	0·39
AR4	504	600	1000	0·24	0·10	0·38
AR5	503	660	950	0·54	0·16	0·41
AR6	539	-	1050**	-	-	-
AR7	539	800	975	1·49	0·26	0·45

* According to the approximate criteria from Peña *et al*[26] and related data from HSM

Table 4 gives these temperatures for the AR glasses and also the results obtained by HSM. The three calculated stability (GS) parameters are given in Table 5: K_{gl} (Hrüby), K_W (Weinberg) and K_{LL} (Lu-Liu). It can be seen that no appreciable differences in GS are detected using K_W and K_{LL} for the glasses investigated here. Only the AR7 glass containing higher levels of P_2O_5 has a large GS index (it is evident that for AR6 glass which has no crystallisation peaks this calculation is not possible; of course it is the most stable glass of the AR series).

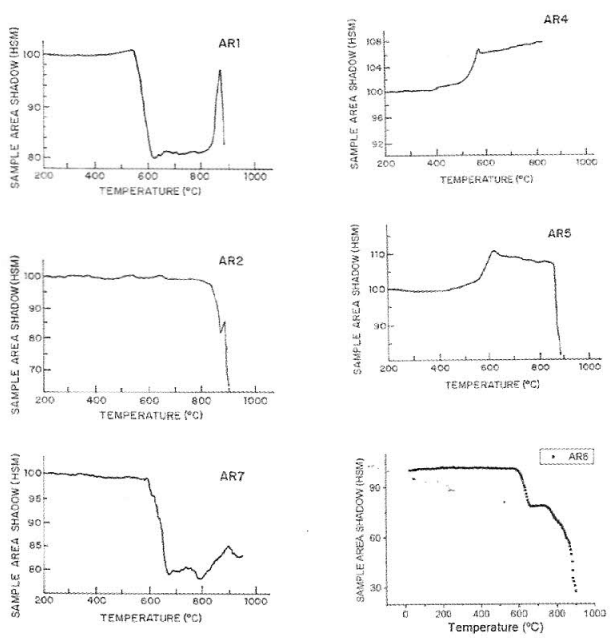

Figure 4. Contraction and expansion on heating of AR iron phosphate series glasses with $UO_{2\cdot67}$ additions measured with HSM apparatus

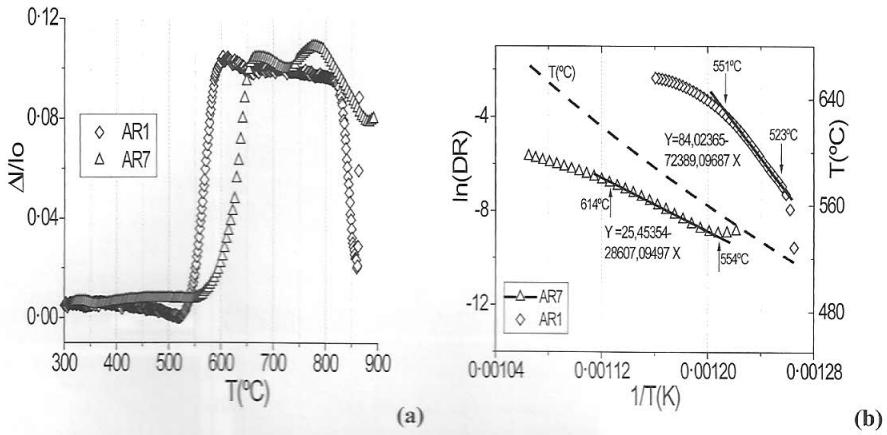

Figure 5. (a) Estimated linear densification in air for AR1 (surface crystallized) and AR7 (bulk crystallised) glass pellets from HSM data and (b) ln(DR) versus 1/T for AR1 and AR7 glass pellets

However, the traditional Hrüby parameter (K_{gl}) used for a long time by many authors[27] does give a major difference in GS for these glasses. Thus, according to these parameters the relative thermal stability of the glasses studied as: AR6>>AR7>AR1>AR5>AR2>AR4.

3.2. Hot stage microscopy (HSM) and physicochemical stability

The pellets for HSM testing were made as follows. The glasses were crushed in a steel mortar. 0·5 g of the glass particles (in iso-propanol media) were ground in an agate mortar (about 7 cm diameter and 3·5 cm depth) for 2 min. Although the particle size distribution was not measured, by this rough method the maximum particle size was in the range 50–75mm. A similar grinding method was applied previously to the $PFeUO_x$ glass reported in Russo *et al.*[21] The pellets were made by axial pressing of the powders with ~2% addition of PVB (polyvinyl butyral, with a molecular weight of ~150000) as a binder.

From the contraction experiments carried out under HSM it can be seen from Figure 4, that AR glasses can be grouped into two classes: glasses that contract and then expand at higher temperatures (AR1, AR7 and AR2) and glasses that just expand (AR4 and AR5). The latter glasses were those which exhibited a greater tendency to crystallisation at high temperatures as shown by DTA (see Figure 3). Table 6 shows the values obtained from these contraction and expansion curves (cross section surface of pellets observed under LCD by HSM).

Table 6. Percentage contraction of sample shadow area from the curves shown in Figure 4

Glass	*% contraction area (T/°C)*	*% expansion (T/°C)*
AR7	20 (660)	7 (900)
AR1	20 (600)	18 (850)
AR2	16 (850) + 35 (875)	Null
AR6	25 (650) + 45 (900)	Null
AR5	30 (850)	15 (610)
AR4	null	6·4 (575)

The expansions (Figure 4, Table 6) for AR4 and AR5 at ~500–600°C are apparently associated with the exothermic-DTA peaks (Figure 3) due to crystallisation of $Fe(PO_4)$ and Fe_2^{3+} $Fe^{2+}(P_2O_7)_2$.[22] Glass AR5 densifies again, probably at its melting point or liquidus.

For AR4 the run was stopped before the fusion temperature was reached. For AR1 and AR7 the densification near T_g is discussed next. For these materials also near probably their melting temperatures a clear expansion is detected which could be associated with a bloating effect provoked by degassing; this must be checked by other techniques (gas chromatography). Further, it is surprising that no densification is seen near their T_g temperatures for AR2, AR4 and AR5.

Figures 5 and 6 show the HSM data for pressed pellets of glasses AR1 and AR7 along with the respective DTA traces. The $\Delta L/L_0$ values were computed from $0{\cdot}5\times\Delta A/A_0$, where $\Delta L=L_0-L(T,t)$ and $\Delta A=A_0-A(T,t)$ where L_0 and A_0 are the initial length

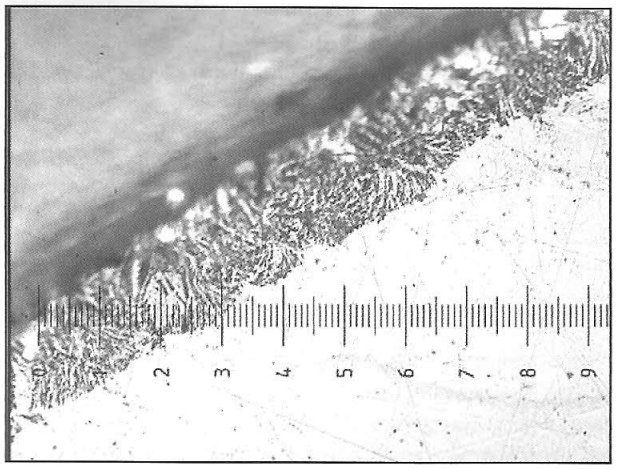

Figure 6. AR1 heated at 630°C for 4 h under O_2 and 672°C for 3 min in air. The polished surface was etched with a given mixture of KOH, H_2O and C_2H_5OH and rinsed in water (Magnification: 2 μm/division) [Colour available online]

and area of the pellet and L and A are the instantaneous length and area of the pellet, being recorded continuously digitally.

With respect to the densification of similar glasses,[21] by comparing both the contraction and DTA traces, a small endothermic peak can be seen at the same temperature where a strong contraction is detected, which is not the case for AR7.

Close agreement is noted between the onset of densification (judged by area reduction) and the DTA determined T_g of the glasses; also the T_g data was discussed before in relation to the dilatometric data shown in Figure 2 and Table 3. At the melting point of the crystalline phases in these glasses a clear expansion in $\Delta A/A_0$ expansion can be seen although this cannot be assigned without ambiguity only to possible density changes. For the case of AR1 the surface crystallisation (internal crystal nucleation/growth is not detected for this glass) involves a type of dendritic or spherulitic crystal. This is shown in Figure 7 and the glass part corresponds to the lower part of the figure.

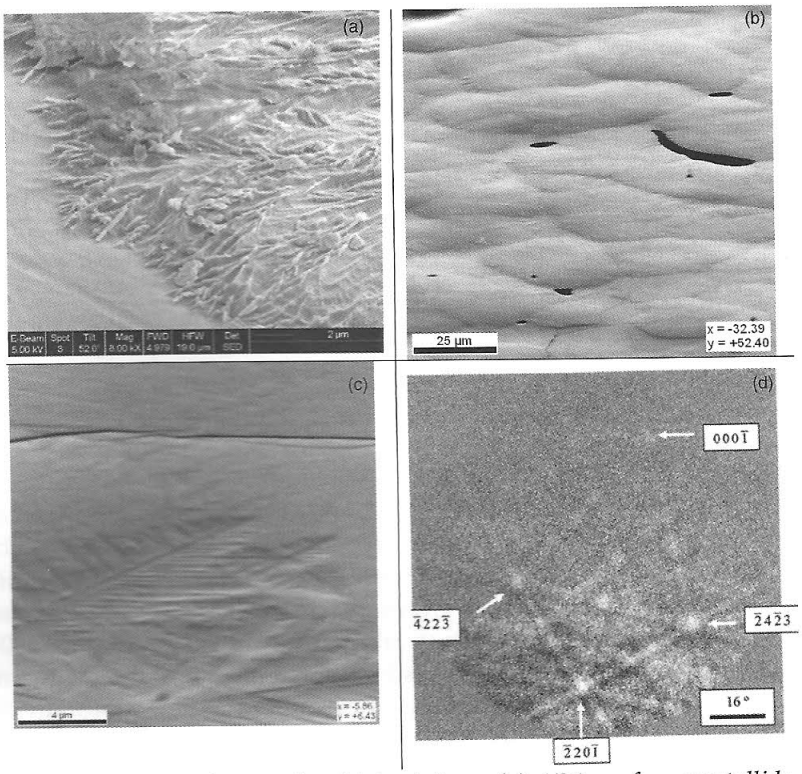

Figure 7. SEM micrographs obtained from: (a) AR1 surface crystallidation, (b) AR4 crystallization between grain boundaries, (c) AR5 (585°C/ 4 h, 0·5°C min^{-1}+650°C) dendritic crystallisation and (d) ESBD diffraction from crystals produced in the AR5 glass after heating at 585+650°C. The pattern corresponds to the dendritic crystals, which are identified as $Fe(PO)_4$ ICSD # 201795 with an hexagonal lattice with a=0·5027 *nm and* c=1·1234 *nm [Colour available online]*

The linear densification $\Delta L(T)/L_0$ versus T(°C) curves for glasses AR1 and AR7 are shown in Figure 5 and it is quite clear AR1 densifies at a lower temperature and with a steeper rise in absolute densification as compared to glass powder AR7. For glasses AR1 and AR7 the main densification continues at temperatures well in excess of the softening point T_s of the glasses. Then the densification rate decreases. Whether the densification is arrested by the probable ongoing crystallisation of the powders needs to be studied.

In principle, the start in densification may be assigned to the Frenkel model for viscous flow sintering[26] based on the glassy particles only. The densification rate may be approximated as

$$\mathrm{DR} = \frac{\mathrm{d}\left(\Delta L(T)/L_0\right)}{\mathrm{d}T} = \frac{s\gamma}{2acA}\exp\left(-\frac{\Delta H_\eta}{RT}\right)$$

where γ is the surface tension and and a is the radius of the assumed spherical particles; c is the heating rate; s is a shape factor with a value of 1 for spherical grains and ~5 for angular crushed particles. The viscosity of the glass may be written as:

$$\eta = A\exp\left(\frac{\Delta H_\eta}{RT}\right)$$

where A contains entropy terms, and ΔH_η is the activation enthalpy for viscous flow. Assuming $s\gamma/2acA$ does not change much with temperature, for a system obeying the above equation a linear relationship between ln(DR) and the variable (1/T(K)) should be obtained. This equation qualitatively describes quite well the early stages of densification of pellets made of glassy grains as seen with a series of cordierite glass compositions.[30]

For the beginning in densification (and up to about 3–4% linear densification; see Figure 5(b)) for both Fe/U phosphate glasses AR1 and AR7 the above linear behaviour is verified for the Frenkel model. The activation enthalpies are 601 and 240 kJ mol^{-1} for AR1 and AR7 and at this stage it is difficult to compare them only in terms of the chemical composition. Glass viscosity values are also be needed. It is also clear that

Table 7. Content of leached elements in the leached filtered liquid after hydrolytic attack of original glasses during 24 h (mg/kg) (according to DIN standard[25] (DIN38414))

Glasses	*P*	*Fe*	*Al*	*Na*
AR5	230	200	5	203
AR1	305	138	9	168
AR2	413	262	15	222
AR6	427	162	10	144
AR4	422	444	12	224
AR7	883	200	33	336
deionised water	0	0	0	0·2

glass AR7 is more viscous than AR1 since both T_g and T_s are higher for AR7 (see Table 3 and Figure 2).

Furthermore, the break in the slopes of the ln(*DR*) versus (1/T) plot can be related either to strong changes in densification mechanisms, as happens in changing from the Frenkel (interconnected pore structure) to the Mackenzie–Shuttleworth (isolated inner porosity) models, or to the onset of crystallisation of the surface and /or the interior part of the glassy grains.

In relation to crystallisation microstructure tendencies (Figure 7(a)–(d)) as discussed previously[23] the interface of surface crystallisation produced in the AR1 glass can be seen clearly by SEM. Figure 8(b) shows the start of surface crystallisation in the grain boundaries of AR4 and Figures 7(c) and (d) show dendritic crystallisation of $FePO_4$ produced in the heat treated AR5 glass and which was identified by EBSD from the polished surface observed under SEM (Figure 7(d)).[23]

It has not been possible to evaluate the fragility of these glass melts, as up to now it has not been possible to obtain low viscosity data for these glasses.[30] Figure 8 shows the glass formation area which can be deduced from results in the AR series glass here investigated and the previous compositions of similar iron phosphate glasses with uranium oxide additions.[23]

In relation to the chemical durability (Table 7) carried out under the standard reported in Magalhaes *et al*[24] for these phosphate glasses (for constant P_2O_5 level of around 54 wt%) the values of 63 (AR1) and 91 (AR2) g m^{-3} suggest that an increase in $UO_{2\cdot67}$, with a similar decrease in the Fe_2O_3 level, increases significantly the corrosion resistance.

The three glasses with highest corrosion resistance AR1 (63 g m^{-3};12·9 wt% UO_2), AR5 (64 g m^{-3};12·5 wt% UO_2) and AR6 (74 g m^{-3}; 18.2 wt% UO_2) have the highest uranium oxide content. However, by comparing AR4 with AR7 it can be seen that an increase of 20% in P_2O_5 and a decrease of 23% in Fe_2O_3 decreases the corrosion resistance by about 31%. As in this case the UO_2 content of 9·1% for AR7 is larger than the 6·2% UO_2 found AR4, the idea that the level of Fe_2O_3 controls the leaching behaviour is still supported. Furthermore, the 5% lower UO_2, about 9% more Fe_2O_3 and 4% lower P_2O_5 for AR1 as compared to AR6, suggests that the higher Fe_2O_3 content (at the expense of a lower P_2O_5 content) explains the higher corrosion resistance of AR1, as suggested in Ojovan & Lee.[31] The present glass compositions based on P-/Fe-oxides, with some of them having important additions of Na_2O, Al_2O_3, and SiO_2, can incorporate significant quantities of UO_2 and still give quite stable glasses from the point of view of chemical durability and crystallisation. This suggests that these matrices can be used for the immobilisation of U radioactive wastes.

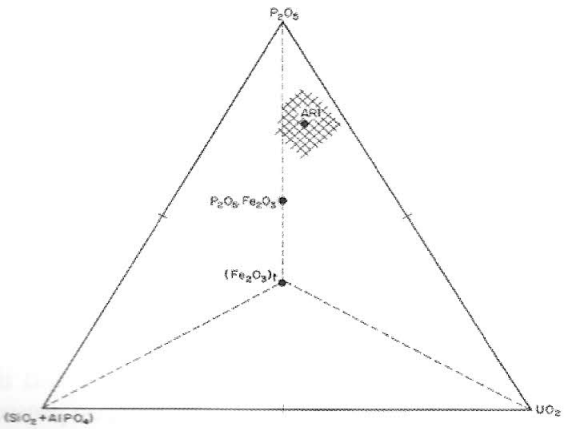

Figure 8. The glass formation area for AR series is outlined in the quaternary diagram by considering the results obtained from the AR glasses and the previous similar iron phosphate glasses previously investigated[20]

Thus, the six examined six glasses can be separated into two groups. One group with a low tendency to crystallisation tendency has compositions with low Fe_2O_3 and high uranium oxide contents (AR1, AR6 and AR7) and relatively high P_2O_5 levels (54% for AR1 and 57-65% P_2O_5 for AR6 and AR7). In this group, AR1 and AR6 exhibited the lowest total water extractions of P, Fe, Al and Na. However, glass AR7 had the lowest chemical resistance and this is apparently related to both a reduced UO_2 level and too high a level of P_2O_5.

The other group contains the remaining glasses AR2, AR4 and AR5 and they show strong crystallisation exotherms at the lowest T_c (crystallisation onset temperature) measured among all the glasses. These compositions have the highest Fe_2O_3 and lowest P_2O_5 contents. More systematic crystal nucleation and growth rate data for these latter glasses may help in understanding such basic processes in iron phosphate glasses containing significant amounts of uranium oxide.

The lower chemical (water leaching) stability of AR5 glass may be due to the presence of glass-in-glass phase separation as detected by DTA, together with its high tendency to crystallize and was not attributed to the uranium content which is very high (12·5%) for this glass. This could be an advantage when these vitreous matrices can be used for immobilizing the U_3O_8 uranium waste.

Future work will involve Raman spectroscopy analysis and nuclear magnetic resonance to elucidate what is the exact role of U_3O_8 in the glass network. Equally, other questions arise: do U and other oxides in the glass, such as lead behave as modifiers of the glass network? With respect to nucleation and crystal growth, more work to determine the TTT curves is in progress. Determination of the mechanical properties of these glasses is also in progress.

Conclusion

A series of new iron phosphate glasses including uranium oxide waste from the CAB, San Carlos de Bariloche, Argentina, have been obtained in the 52–77 wt% P_2O_5 range and 22–48 wt% Fe_2O_3 ranges (named AR glasses) with inclusion of 6·6 to 19·4 wt% of $UO_{2\cdot67}$. The final glasses are homogeneous, shiny, black and do not show crystallised areas by eye as the uranium oxide is well dissolved in the vitreous matrix.

Thermal expansion experiments from these glasses give TEC values of $2\cdot6–10\cdot8\times10^{-6}$ °C^{-1} with T_g=493–539°C and T_s=526–589°C. From these data and the DTA traces, as well as HSM experiments on pressed powdered glasses, it has been possible to evaluate the Hrüby (K_{gl}), Weinberg (K_W) and Li–Liu (K_{LL}) glass stabilisation (*GS*) parameters. It is concluded that K_{gl} provides the best representation of thermal stability differences among these AR glasses. AR2, AR4 and AR5 glasses which have higher Fe_2O_3 contents show the greatest tendency to crystallize with several exothermic peaks observed by DTA. The AR6 and AR7 glasses, with higher P_2O_5 contents are the most stable glasses against crystallisation. Crystallisation of these glasses increases with iron oxide content and decrease with uranium content; that is, glasses containing more $UO_{2\cdot67}$ are the more thermally stable glasses.

Conversely, with respect to water durability glasses with higher P_2O_5 contents have a less stable glass network because they release more components of the glass into water, namely P, Al, Fe and Na. Thus, the least chemically (water) durable composition was AR7 and the most durable were AR5 and AR1. These latter glasses are less thermally stable, in the case of AR1 this is because of its tendency to undergo surface crystallisation. No relation between the water durability and the $UO_{2\cdot67}$ content has been found. It seems that the glass with the highest uranium oxide content (AR6) is the most thermally stable and that the amounts of the leached components from this glass are acceptable compared to the values obtained for other iron phosphate glasses of this AR series.

Acknowledgement

J. Ma. Rincon thanks IAEA, Vienna, Universidad Nacional de Cuyo, the Joint European Master Programme on Advanced Materials Science and Engineering and FP7-IRSES Project Nr. 247524 'NanoCom Network' for financial support. The authors thank Carlos Cotaro, Ernesto Scerbo and Carolina Ayala [Centro Atómico Bariloche (CAB)] for the SEM work and EDS/EDAX analysis. Financial support of the Centro Atómico Bariloche Superconductivity Group, which made possible the purchase of the main dilatometer components is acknowledged.

References

1. Robredo, J. Le verre dans la technologie nucléaire. *Verres Réfract.*, 1964, 3-13
2. Romero M. & Rincón, J. Ma. *Bol. Soc. Esp. Ceram. Vidr.* , 2001, **39** (1), 155.
3. Ballesteros, S., Parga, J. & Rincón, J. Ma. Vitrificación para inmovilizar residuos peligrosos. *Cie. Desarrollo*, 2010, **243** (36), 6–11.
4. Hidalgo, M. & Rincón, J. Ma. *Bol. Soc. Esp. Ceram. Vidr.*, 1987, **26**, (4), 227.
5. Ojovan, M. I. & Lee, W. E. *Metall. Mater. Trans. A*, 2011, **42A**, 837–51.
6. Bonnet, P. & Millet, J. M. M. *J. Catal.*,1996, **161**, 198.
7. Jantzen, C. M. *J. Non-Cryst. Solids*, 1986, **84**, 215.
8. Yu, X., Day, D. E., Long G. J. & Brow, R. K. *J. Non-Cryst. Solids*, 1997, **215**, 21–31.
9. Mesko, M. G. & Day, D. E. *J. Nucl. Mater.*, 1999, **273**, 27–36.
10. Ray, C. S., Fang, X. Karabulut, M., Marsinghe, G. K. & Day, D. E. *J. Non-Cryst. Solids*, 1999, **249**, 1–16.
11. Bingham, P. A. , Hand, R. J. & Forder, S. D. *Mater. Res. Bull.*, 2006, **41**, 1622
12. Jantzen, C. M., Kaplan, D. I., Bibler, N. E., Peeler, D. K. & Plodinec, M. J. *J. Nucl. Mater.*, 2008, **378**, 244.
13. Marasinghe, G. K., Karabulut, M., Ray, C. S., Day, D. E., Shumsky, M. G., Yelon, W. B., Booth, C. H., Allen, P. G. & Shuh, D. K. *J. Non-Cryst. Solids*, 1997, **222**, 144–52.
14. Bingham, P. A., Hannant, O. M., Hand, R. J., Forder, S. D. & Hyatt, N. C. Modified iron phosphate glasses for waste inmobilisation: advantages and limitations. *Crystallisation*, Foz do Iguazú, Sept., 2009, 0088.
15. Zhang, L., Ghussn, L. Schmidtt, M. L., Zanotto E. D., Brow, R. K. & Schlesinger, M. E. *J. Non-Cryst. Solids*, 2010, **356**, 2965–8.
16. Zhang, L., Schlesinger, M. E. & Brow, R. K. *J. Am. Ceram. Soc.*, 2011, **94** (5), 1605–10.
17. Russo, D. O., Rodríguez, D. S., Sterba, M. N., Rincón, J. Ma. & González Oliver, C. J. R. In *Jornadas Sam/Conamet/AAS Argentina*. Edited by SAM-CONAMET, 2001, P 835.
18. Russo, D. O., Rodríguez, D. S., Grumbaum, N. & González Oliver, C. J. R. In: *Jornadas Sam/Conamet/Simposium Materia*, Argentina. Edited by SAM-CONAMET., 2003, 12-04, 995–8.
19. Villegas, Mª. A., Rincón, J. Ma., Russo, D. & González- Oliver, C. J. R. *VARIREI 2005*, University of LÁquila, RCG 6, 2005, **Vol. 1,** P 6.
20. Gonzalez-Oliver, C. J. R. Russo, D., Lovey, M. & Rincón, J. Ma. In *XIII Ann. Meeting SME*. Edited by Soc. Esp. Microscopia, Bilbao. Mat., 2007, P38.
21. Russo, D. O., Rodríguez, D. S., Rincón L., J. Ma., Romero, M. & Gonzalez- Oliver, C. J. R. *J. Non-Cryst. Solids*, 2008, **354**, 1541–8.
22. Gonzalez-Oliver, C. J. R., Russo, D. O., Lovey, F. C., Romero, M. & Rincón, J. Ma., Iron aluminium silico-phosphate glasses including U_3O_8. In: *Scientific Basis for Nuclear Waste Management XXXIII*. Eds B. E. Burakov & A. S. Aloy. *Mater. Res. Soc. Symp. Proc.* 2009, **1193**, 329–36.
23. Gonzalez- Oliver, C. J. R., Lovey, F. C., Caneiro, A. Russo, D. O., Rodriguez, D. S., Soldera, F., Fiscina, J. E. & Rincon J. Ma. *J. Non-Cryst. Solids*, 2010, **356**, 2986
24. Magalhaes, J. M. & Silva, J. E. Effect of experimental inertization of galvanic sludges in ceramics. *J. Hazard. Mater.*, 2004, **106B**, 139–47.
25. Romero, M., Hernández- Crespo, M. S. & Rincón, J. Ma., Leaching behaviour of a glassy slag and derived glass ceramics from arc plasma vitrification of hospital wastes. *Adv. Appl. Ceram.*, 2009, **108**, 67–71.
26. *Standard test methods for determining chemical durability of nuclear, hazardous and mixed waste glasses and multiphase glass ceramics: The product consistency test (PCT).* ASTM C1285-02, 2008.
27. Pérez, J. M. , Romero, M. & Rincón, J. Ma. *DTA/ DSC Applied to Study of Glass-To-Glass-Ceramic Transformation in Glasses From Wastes*. 2011, Edited by Research Signpost, 37/661(2), Vazhappalli Jn., Fort Post Office, Trivandrum-695 023, Kerala, India, 2011.
28. Scholze, H. Influence of viscosity and surface tension on hot-stage microscopy measurements on glasses. *Ver. Dtsch. Keram. Ges.*, 1962, **391**, 63–8.
29. Fernández-Navarro, J. Mª. *El Vidrio Second Edition*, CSIC, Madrid, 2001.
30. Peña, R, Rubio, J., Rubio, F., Oteo, J. L., Rodrigo, J. L. & Ferrando V., Puntos característicos de vidriados cerámicos determinados por ATDs, in: *Qualicer 2004*. Edited by Cámara de Comercio e Industria de Castellón. pp. 31–5.
31. Ojovan, M. & Lee, W. E. Connectivity and glass transition in disordered oxide systems. *J. Non-Cryst. Solids*, 2010, **356**, 2534–40.
32. García, L.F., Malachevsky, M. T., Fiscina, J. E. & Gonzalez- Oliver, C. J. R. *Phys. Chem. Glasses*, 2002, **43C**, 466–70.